IMMUNOLOGY

The mechanosensitive channel TRPV4 inhibits pulmonary inflammation by limiting NF-κB signaling in alveolar macrophages

Adam M. Boulton[1]†, Megan E. Grund[1]†, Yuxin Wang[1], Erica M. Orsini[2], Yan Liu[1], Susamma Abraham[1], Lisa M. Grove[1], Ryan Musich[1], Caitlin M. Snyder[1], Haley Ricci[1], Amber Cardani-Boulton[3], Vidula Vachharajani[1,2], Mitchell A. Olman[1,2], Rachel G. Scheraga[1,2]*

The nuclear factor κB (NF-κB) signaling pathway plays a critical role in activating macrophages in the pathogenesis of many inflammatory diseases. Tissue mechanical properties are important in modulating key cellular proinflammatory responses. Here, we investigated how the mechanosensitive membrane cation channel TRPV4 (transient receptor potential vanilloid 4) limits macrophage proinflammatory responses in bacterial pneumonia. We found that TRPV4 suppressed proinflammatory gene expression in alveolar macrophages in response to *Pseudomonas aeruginosa* pneumonia in mice and in response to agonists of various Toll-like receptors (TLRs) in vitro. TRPV4 suppressed proinflammatory gene expression in macrophages by decreasing the activity of the NF-κB subunit p65. Upon stimulation of macrophages with bacterial lipopolysaccharide, a fraction of TRPV4 translocated from the endoplasmic reticulum to the plasma membrane, releasing p65 for nuclear translocation. TRPV4 interacted with p65 through an N-terminal cytoplasmic ankyrin repeat domain (ANKRD) that shares sequence homology with the p65-binding ANKRD of the NF-κB inhibitor IκBα. Given the diverse roles of TRPV4 and NF-κB in various cell types, our identification of cross-talk between a mechanosensitive channel and p65 in macrophages suggests application to many NF-κB–dependent diseases, such as cancer and atherosclerosis.

INTRODUCTION

Bacterial pneumonia is one of the leading causes of hospitalization, morbidity, and mortality in the United States (*1*). Bacterial pneumonia progresses to acute lung injury or acute respiratory distress syndrome (ARDS) in ~31% of patients, leading to worse patient outcomes (*2*, *3*). Direct injury to the lung by bacterial pneumonia is mediated in part by the proinflammatory cytokine response in the alveolar space (*3*–*5*). A milieu of proinflammatory factors such as chemokines CXCL1, CCL2, and CCL3 attracts monocytes, macrophages, and neutrophils, accelerating lung tissue damage (*6*, *7*). Macrophages are key innate immune cells in the lung that secrete additional cytokines and chemokines (*7*). Thus, it is important to understand in detail the mechanism(s) by which macrophages tightly limit the transcription of proinflammatory factors in response to the alveolar lung microenvironment.

Macrophage populations patrol and migrate into the lung after injury or infection (*8*). Emerging research highlights the distinct roles of lung macrophage populations, including tissue-resident alveolar macrophages (TR-AMs), which express the immunoglobulin-like lectin Siglec-F, and monocyte-derived or recruited alveolar macrophages (Mo-AMs), which down-regulate Siglec-F expression (*9*). The mechanical signals from the lung microenvironment influence the macrophage population diversity and may stimulate signaling that controls its activation functions (*10*). Clues to the mechanistic plasticity of TR-AMs and Mo-AMs come from the cancer and aging literature, with the discovery of unique gene signatures associated with the changing lung microenvironment, but less is known about this plasticity during infection (*11*, *12*). During infection or tissue inflammation, macrophage activation occurs through the recognition of pathogen-associated molecular patterns (PAMPs) by pattern recognition receptors (PRRs) such as the Toll-like receptor (TLR) family members (*13*). TLRs are located primarily within the plasma membrane (for example, TLR1/2 heterodimers and TLR4) or on intracellular endosomes (TLR3 and TLR9) (*14*, *15*). Stimulation of TLRs by PAMPs, such as lipopolysaccharide (LPS) or nucleic acids, activates inflammatory signaling cascades, most notably the nuclear factor κB (NF-κB) pathway. As such, the NF-κB pathway is a master regulator of proinflammatory gene transcription, playing an important pathogenic role in infection, inflammation, and malignancy (*16*). The NF-κB pathway is a network of classical and alternative activators and inhibitors allowing for a tightly regulated cascade of signals leading to transcription of proinflammatory cytokines after PAMP activation. However, the putative convergent signals from the stiffened microenvironment are less characterized (*16*). Four decades of research have defined essential partners, interacting motifs, and environmental cues to activate and inhibit the NF-κB pathway (*17*, *18*), which may be influenced uniquely in tissues sensitive to mechanical strain and stress such as the lung.

Transient receptor potential vanilloid 4 (TRPV4) is a mechanosensitive cation membrane channel that is capable of both "outside-in" and "inside-out" signaling in a cell type–specific and context-specific manner. TRPV4's bidirectional signaling is a consequence of multiple stimuli, including intracellular calcium ions (Ca^{2+}), the activation of intracellular kinases, and/or the direct interaction with cytoskeletal proteins through its intracellular N-terminal and C-terminal tails (*19*–*21*). TRPV4 has both Ca^{2+}-dependent and Ca^{2+}-independent

[1]Inflammation and Immunity, Cleveland Clinic Research, Cleveland Clinic Foundation, Cleveland, OH 44106, USA. [2]Integrated Hospital Care Institute, Department of Pulmonary and Critical Care, Cleveland Clinic Foundation, Cleveland, OH 44106, USA. [3]Neuroscience, Cleveland Clinic Research, Cleveland Clinic Foundation, Cleveland, OH 44106, USA.
†These authors contributed equally to this work.
*Corresponding author. Email: scherar@ccf.org

functions (*22*). TRPV4 is activated by both chemical [for example, 6-epoxyeicosatrienoic acid (EET) and 4α-phorbol 12,13-didecanoate (4-αPDD)] and physical (for example, stretch and stiffness) stimuli. Our previous work shows that TRPV4 is essential for macrophage phagocytosis and anti-inflammatory cytokine secretion in response to LPS in vivo and in vitro (*23*). Furthermore, in a clinically relevant model of chronic *Pseudomonas aeruginosa* pneumonia, TRPV4 protects against lung injury by switching LPS-induced mitogen-activated protein kinase (MAPK) signaling from the primary MAPK c-Jun N-terminal kinase (JNK) to that of MAPK p38 (*24*).

Here, we aimed to identify the molecular mechanism in alveolar macrophages by which TRPV4 suppressed proinflammatory cytokine production and limited lung injury in the acute *P. aeruginosa* pneumonia model in vivo and TLR agonism in vitro. We showed that alveolar macrophage–specific *Trpv4* knockout (KO) mice had increased proinflammatory cell infiltration and lung injury, and the recruited macrophage population in these mice had increased proinflammatory cytokine abundance in vivo. In response to agonists of TLR1/2, TLR4, and TLR9, TRPV4 restrained excessive proinflammatory gene expression in vitro. The suppression of proinflammatory gene expression was found to be through the binding of the TRPV4 ankyrin repeat domain (ANKRD) to p65, the subunit of the NF-κB complex that translocates to the nucleus and acts as a transcriptional activator upon NF-κB activation. Moreover, the ANKRD of TRPV4 shares sequence homology with the ANKRD of the NF-κB pathway inhibitor IκBα. Upon stimulation with LPS, a fraction of TRPV4 dissociated from the NF-κB complex, translocating from the endoplasmic reticulum (ER) to the plasma membrane, whereas the free fraction of p65 translocated to the nucleus, driving the transcription of genes encoding proinflammatory cytokines. However, the residual TRPV4 on the ER membrane sustained interaction with p65 to limit maximal proinflammatory cytokine transcription. Together, these data suggest that targeting the molecular interaction between TRPV4 and p65 may inhibit macrophage activation to limit lung injury in vivo in an infected lung microenvironment.

RESULTS

TRPV4 in monocyte-derived alveolar macrophages limits proinflammatory cytokine gene expression in response to *P. aeruginosa* pneumonia

Our previous work has shown that global *Trpv4* KO mice develop more severe lung injury and decreased bacterial clearance upon chronic infection with agarose-embedded *P. aeruginosa* compared with wild-type (WT) mice (*24*). Furthermore, alveolar macrophages are the key phagocytic cell and likely source of proinflammatory cytokines such as interleukin-6 (IL-6) and the CXC family chemokines CXCL1 and CXCL2 (*24*). To address whether TRPV4 loss in macrophages is responsible for the increased lung inflammation in *Trpv4* global KO mice, we generated alveolar macrophage–specific *Trpv4* KO mice (*Cd11c*Cre: *Trpv4*$^{fl/fl}$), which have genetic deletion of TRPV4 in all alveolar macrophage populations (TR-AMs and Mo-AMs) (*25*, *26*). Free, live *P. aeruginosa* (not agarose-embedded) was then intranasally administered to mice to model acute pneumonia (Fig. 1A). Compared with parental controls (*Trpv4*$^{fl/fl}$), alveolar macrophage–specific *Trpv4* KO mice (*Cd11c*Cre:*Trpv4*$^{fl/fl}$) had increased lung injury, as measured by increased neutrophil and decreased macrophage recruitment to the alveolar space (Fig. 1B); significantly increased CCL3 secretion; and a trend toward increased CXCL1 in the bronchoalveolar lavage fluid (BALF) (Fig. 1C). Also, recruited alveolar macrophages (Mo-AMs; CD45^{+}F4/80^{+}Siglec-F^{-}) isolated by collagenase digestion of whole lung homogenate exhibited increased CCL2 and IL-1β protein abundance in alveolar macrophage–specific *Trpv4* KO mice compared with controls (Fig. 1, D and E, and fig. S1). Overall, these data suggest that TRPV4 in Mo-AMs is necessary for the lung injury response driven by cytokine and chemokine production in these cells.

TRPV4 negatively regulates the expression of NF-κB–responsive genes

A previous work shows that TRPV4 promotes the activation of alveolar and bone marrow–derived macrophages (BMDMs) in a matrix substrate–dependent manner, promoting phagocytosis and reducing proinflammatory cytokine secretion (*23*). In addition, both macrophage TRPV4 and TLR4 mediate inflammation through a JNK-p38 molecular switch (*24*). To determine the mechanism by which TRPV4 limits macrophage proinflammatory signaling, we measured proinflammatory cytokine transcripts in WT and *Trpv4* KO BMDMs stimulated with the TLR agonists Pam3CSK4 (TLR1/2), LPS (TLR4), polyinosinic:polycytidylic acid (poly I:C) (TLR3), and CpG DNA (TLR9). We measured the changes over time (1 and 6 hours) because changes in gene expression downstream of these TLRs are different between TLRs. Loss of TRPV4 increased *IL-1*β and *Cxcl1* induced by the TLR4 agonist by twofold and increased *Cxcl1* induced by the TLR1/2 agonist by 1.5-fold at 1 hour (Fig. 2A). However, at 6 hours, loss of TRPV4 significantly increased *Cxcl1* induced by either the TLR4 or TLR9 agonists by twofold with a trend to increase with the TLR1/2 agonist (Fig. 2B). This provides a broad response of the TRPV4 signal integration to plasma membrane TLRs early and endosomal TLRs later with tissue mechanical signals.

Given that TRPV4 attenuated the proinflammatory transcriptional response more robustly early (1 hour) after stimulation with the plasma membrane TLR4 agonist LPS, the mechanism of TRPV4 action was explored specifically using LPS. We performed single-cell sequencing in WT and *Trpv4* KO BMDMs ± LPS. Nine macrophage clusters were identified and annotated on the basis of differentially regulated genes that reflect dissimilar phenotypic groups of macrophages (Fig. 2C). Many NF-κB–regulated genes were differentially expressed, consistent with the fact that TRPV4 can stimulate molecular switching between JNK and p38, both of which activate the NF-κB pathway (*24*). The *IL-1*β+_*Cxcl2*+ cluster had the greatest difference in NF-κB–dependent genes (https://bu.edu/nf-kb/gene-resources/target-genes/) upon comparison of BMDMs ± TRPV4 (*27*). In this cluster, TRPV4 KO in BMDMs resulted in substantial changes in key NF-κB–regulated pathways, both with and without LPS, as analyzed by gene ontology enrichment analysis (GO:BP gene pathway analysis) (Fig. 2D and fig. S2, A to C). Furthermore, genes in the *IL-1*β+_*Cxcl2*+ cluster from *Trpv4* KO BMDMs (15 to 30% of the total population) showed an increased inflammatory response under basal and TLR4 agonist conditions, as compared with WT BMDMs (Fig. 2D and fig. S2C). Key genes in the defense response pathway genes in this cluster included *Ccl4*, *Ccl7*, *Ccl2*, *Apoe*, *Cxcl10*, *Lpl*, *Rsad2*, and *Ccl3*. Hence, TRPV4 did not drive formation of a previously unobserved macrophage population, but rather the presence of TRPV4 was important in a specific cluster of macrophages to reduce the NF-κB–dependent proinflammatory pathway (Fig. 2, C

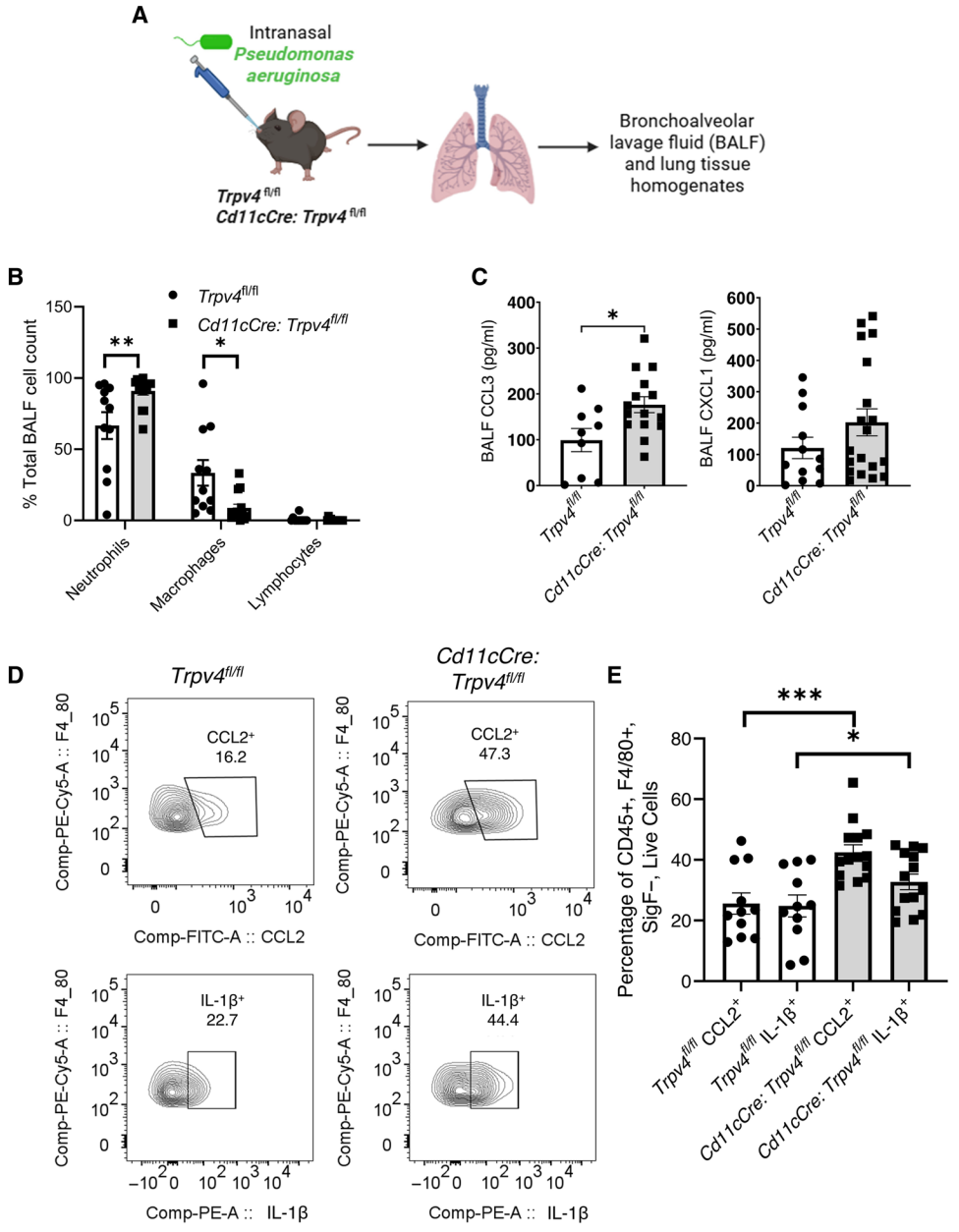

Fig. 1. TRPV4 in monocyte-derived alveolar macrophages protects the lung from injury by limiting p65-dependent cytokine expression in vivo. (**A**) Schematic of *P. aeruginosa*–induced pneumonia mouse model. Cells were collected from BALF and lung tissue homogenates in alveolar macrophage–specific *Trpv4* KO mice (*Cd11c*Cre:*Trpv4*$^{fl/fl}$) and parental controls (*Trpv4*$^{fl/fl}$). Created with BioRender. (**B**) Percentage of neutrophils, macrophages, and lymphocytes in BALF. $n = 14$ or 15 mice per group. $^{*}P \leq 0.05$; $^{**}P \leq 0.01$, by Student's *t* test. (**C**) Quantification of CCL3 and CXCL1 in BALF from *Trpv4*$^{fl/fl}$ and *Cd11c*Cre:*Trpv4*$^{fl/fl}$ mice by LEGENDplex. $n = 14$ or 15 mice per group. $^{*}P \leq 0.05$, by Student's *t* test. (**D**) Lung tissue homogenates were subjected to flow cytometry with gating on percent CD45^{+}F4/80^{+}SiglecF^{-} populations for IL-1β and CCL2 in *Cd11c*Cre:*Trpv4*$^{fl/fl}$ and *Trpv4*$^{fl/fl}$ mice. (**E**) Quantification of CCL2^{+} and IL-1β^{+} alveolar macrophages (CD45^{+}F4/80^{+}SiglecF^{-}). $n = 14$ or 15 mice per group. $^{*}P \leq 0.05$; $^{***}P \leq 0.001$, by Student's *t* test.

and D). This phenomenon explains the heterogeneous and modest proinflammatory cytokine response to TLR agonism in the BMDM population as a whole (Fig. 2, A and B).

TRPV4 limits p65 transcriptional activity and cytokine secretion

To further understand how TRPV4 limits NF-κB–dependent expression of cytokine transcripts, we investigated NF-κB function using a NF-κB response element luciferase assay in HeLa cells, which respond to LPS and are easily transfected. Overexpression of TRPV4 led to decreased NF-κB promoter activity in both untreated and LPS-treated cells as compared with cells expressing empty vector (EV) (Fig. 3A). To confirm this finding, BMDMs from mVenus-RELA reporter mice were used to show abundance of Rela (p65), which is a direct transcriptional target of NF-κB (*28*). Similarly, we found down-regulation of TRPV4 with small interfering RNA (siRNA) (60 to 70% knockdown) in mVenus-RELA BMDMs with and without LPS increased fluorescence by flow cytometry compared with controls, indicating that TRPV4 protein abundance decreased expression of the p65 target gene (Fig. 3A and fig. S3A). Together, these data suggest that TRPV4 is required to limit p65 transcriptional activity under basal and LPS-stimulated conditions. In agreement with our previous report that TRPV4 is required for IL-1β secretion upon LPS stimulation (*23*), we found that siRNA-mediated knockdown of p65 reduced LPS-induced IL-1β secretion in both *Trpv4* KO BMDMs and WT BMDMs, indicating that *Trpv4* KO induction of IL-1β is due to p65 transcriptional activity (Fig. 3B; 60 to 70% knockdown; fig. S3B). Together, these data demonstrate that TRPV4 inhibits NF-κB signaling in a p65-dependent manner.

TRPV4 stabilizes IκBα and limits p65 translocation to the nucleus

When cells receive an inflammatory stimulus, such as LPS, phosphorylation of the NF-κB inhibitor IκBα by the IκB kinase subunit β (IKK-β) leads to the degradation of IκBα, leading to translocation of p65 into the nucleus, where it stimulates the expression of target genes (*29*). To determine the mechanism whereby TRPV4 blocks NF-κB pathway activation, we measured IκBα degradation, an essential step for transcription of genes encoding proinflammatory cytokines, after LPS treatment (Fig. 3C). In the absence of TRPV4, IκBα was degraded two times faster (5 to 10 min in *Trpv4* KO versus 20 min in WT) (Fig. 3C). This faster IκBα degradation seen in the *Trpv4* KO was independent of TRPV4-mediated Ca^{2+} signaling because degradation was not significantly different in the presence of a TRPV4-specific Ca^{2+} inhibitor, HC-067047 (fig. S4). The increased IκBα degradation in *Trpv4* KO BMDMs was

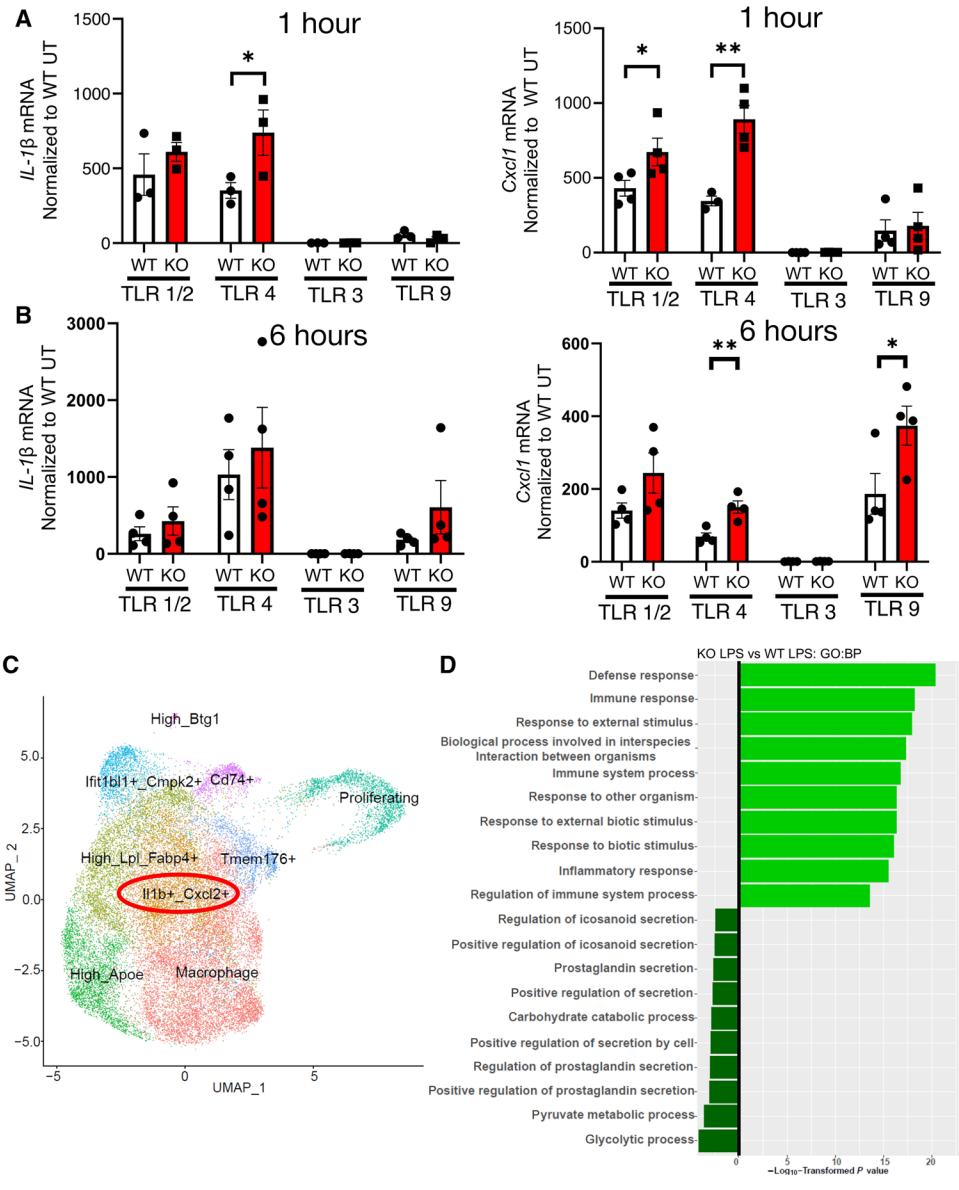

Fig. 2. TRPV4 negatively regulates TLR-induced expression of cytokine transcripts in a subset of BMDMs with high expression of NF-κB–dependent genes. (**A** and **B**) Quantification of *IL-1β* and *Cxcl1* transcripts 1 hour (A) and 6 hours (B) after stimulation of BMDMs from WT and *Trpv4* KO mice with TLR agonists. Transcript amounts were normalized to those in untreated BMDMs from WT mice (WT UT). TLR agonists: TLR1/2 (Pam3CSK4, 100 ng/ml), TLR4 (LPS, 100 ng/ml), TLR3 (Poly I:C, 10 μg/ml), and TLR9 (CpGDNA, 5 μg/ml). $n = 3$ or 4 biological replicates per group. $^*P \leq 0.05$; $^{**}P \leq 0.01$, by Student's *t* test comparing *Trpv4* KO versus WT BMDMs within a TLR agonist treatment group. (**C**) UMAP cluster plot shows nine clusters in WT and *Trpv4* KO BMDMs ± LPS after 10X Genomics. $n = 3$ biological replicates per group. (**D**) GO BP gene pathway analysis within the $Il1\beta^+\_Cxcl2^+$ cluster in (C) comparing LPS-stimulated cells from WT and KO mice showing significant represented pathways as measured by $-\log_{10}$ transformed *P* value (*x* axis; light green: increased KO versus WT; dark green: decreased KO versus WT).

accompanied by an increase in p65 translocation to the nucleus after LPS (30 min) compared with WT BMDMs (Fig. 3D), further implicating TRPV4 as a negative regulator of p65-dependent transcription. Overall, TRPV4 inhibited NF-κB function through limiting IκBα degradation and p65 translocation to the nucleus.

The TRPV4 N-terminal domain has sequence homology and conservation with the binding interface between IκBα and p65/p50

TRPV4 has N-terminal and C-terminal tails residing in the cytoplasm that bind to intracellular signaling molecules, driving cellular functions (*30*, *31*). Hence, we next explored whether the mechanism by which TRPV4 limits IκBα degradation and p65 translocation was through direct binding to p65. The ANKRD domain of IκBα interacts with the p65 Rel homology domain, specifically with the IPT (Ig-like, plexins, transcription factors) domain. Because TRPV4 contains an ANKRD domain, we assessed the sequence homology between IκBα ANKRD and TRPV4 ANKRD to determine whether TRPV4 binding to p65 might explain the delay in p65 translocation to the nucleus upon LPS stimulation (*32*–*34*). Sequence analysis revealed that the TRPV4 N-terminal cytoplasmic tail has an ANKRD similar to that of IκBα. Using the CLC Genomics Workbench (Qiagen), the TRPV4 N terminus was aligned with the p65 interaction domains (N-terminal Rel homology domain and C-terminal Rel homology domain or referred to as the IPT domain) showing ANKRD similarity (>50%) to IκBα at the interaction interface with p65/p50, which have the potential to participate in protein-protein interactions (Fig. 4A) (*33*). Next, IκBα residues that were similar to the TRPV4 N-terminal tail were selected to model the interaction with p65 and p50 (Fig. 4A). The IκBα-p65/p50 binding that contributes to strong interacting forces includes electrostatic, hydrophobic, and aromatic π-π stacking forces (Fig. 4A). Because the published structure of human IκBα is in a complex with a heterodimer of p65 and p50, the key interactions are shown with both p65 and p50 (Fig. 4A) (*32*). Together, these data suggested that TRPV4 bound to p65 in a similar manner as IκBα, thereby negatively regulating the NF-κB pathway.

TRPV4 binds to p65 in the NF-κB complex under both untreated and LPS-treated conditions

To determine whether TRPV4 and p65 interact biochemically, we performed coimmunoprecipitation assays using both a TRPV4 overexpression system and an endogenous system. TRPV4 and p65 interacted when both were overexpressed in 293T (Fig. 4B) and HeLa cells (fig. S5), and immunoprecipitation of endogenous p65 pulled down TRPV4 in WT BMDMs but not in *Trpv4* KO BMDMs (Fig. 4C). Interaction between TRPV4 and p65 was observed in both the basal and LPS-stimulated states (Fig. 4C), demonstrating the ability of

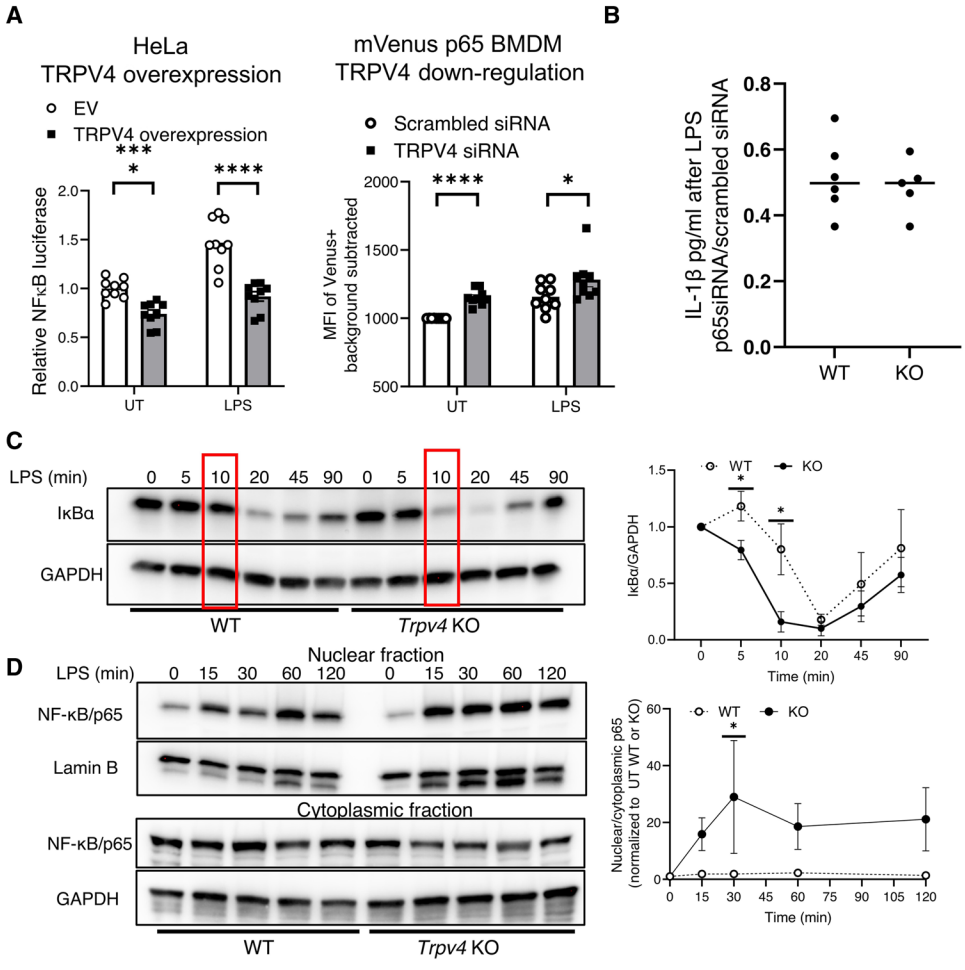

Fig. 3. TRPV4 negatively regulates p65-responsive promoter activity by stabilizing IκBα and limiting p65 nuclear translocation. (**A**) The transcriptional activity of NF-κB response elements was evaluated in HeLa cells cotransfected with an NF-κB response element luciferase reporter and either EV or TRPV4 plasmid (TRPV4 overexpression) ± LPS (100 ng/ml, 16 hours) and in BMDMs from mVenus-RELA (p65) reporter mice transfected with either control (Scrambled) siRNA or TRPV4 siRNA ± LPS (1 μg/ml, 1 hour). For HeLa TRPV4 overexpression, $n = 3$ biological replicates per group. ****$P \leq 0.0001$, by Student's t test. For mVenus p65 BMDM, $n = 5$ biological replicates per group. *$P \leq 0.05$; ****$P \leq 0.0001$, by Student's t test. (**B**) Quantification of IL-1β in the conditional medium of BMDMs from WT and *Trpv4* KO mice that were transfected with control (Scrambled) or p65 siRNA and treated with LPS (100 ng/ml, 24 hours). IL-1β amounts are presented as relative to the value in cells not treated with LPS. $n = 6$ biological replicates per group. Student's t test shows no statistical difference. (**C**) BMDMs from WT and *Trpv4* KO mice were treated with LPS in the indicated time course, and the amount of IκBα was determined by immunoblotting. GAPDH is a loading control. $n = 3$ biological replicates per group. *$P \leq 0.05$, by Student's t test. Red boxes highlight the time point at which degradation begins to significantly deviate between WT and *Trpv4* KO BMDMs. (**D**) BMDMs from WT and *Trpv4* KO mice were treated with LPS in the indicated time course, and the nuclear and cytoplasmic fractions were immunoblotted for p65. The amount of p65 in the nuclear fractions (red box) was quantified. $n = 3$ biological replicates per group. *$P \leq 0.05$, by Student's t test.

TRPV4 and p65 to bind and thereby suppress LPS-stimulated inflammation in macrophages. To determine the approximate location of TRPV4 and p65 before and after LPS stimulation, immunofluorescence was performed on *Trpv4* KO BMDMs transduced with lentivirus (LV) carrying Myc-tagged full-length (FL) TRPV4 (Myc-TRPV4^{FL}) (Fig. 4D). TRPV4 and p65 colocalized in the cytoplasm of *Trpv4* KO BMDMs, but colocalization was reduced upon LPS stimulation, as determined by Pearson's coefficient (Fig. 4D). Furthermore, p65 staining in the nucleus increased upon LPS stimulation as assessed by Pearson's coefficient of p65 and nuclear 4′,6-diamidino-2-phenylindole (DAPI) staining (Fig. 4D). Similarly, the TRPV4 and p65 complex colocalized in close proximity to the perinuclear region in HeLa cells, as shown using an irreversible bimolecular fluorescence complementation assay in cells transfected with TRPV4 and p65 tagged with the N-terminal and C-terminal domains of Venus (VN and VC), respectively (Fig. 4, E and F). Together, these data provided supportive evidence of a biochemical interaction, as well as colocalization of TRPV4 and p65 by multiple methods in both overexpression and endogenous expression systems.

The N-terminal ANKRD domain of TRPV4 mediates binding to p65

Because multiple methods indicated that TRPV4 and p65 interact, we investigated which region of TRPV4 bound to p65. Given its sequence homology to IκBα, the N-terminal ANKRD of TRPV4 was predicted to interact with p65. Therefore, the ANKRD of TRPV4 was deleted (hTRPV4$^{\Delta ANKRD}$ or TRPV4$^{\Delta ANKRD}$) to determine whether p65 binding was abrogated. The NanoBiT protein-protein interaction structural complementation reporter system was used as follows: The large (Lg) BiT sequence was fused to either FL hTRPV4 (LgBiT-TRPV4^{FL}) or ANKRD-deleted TRPV4 (LgBiT-TRPV4$^{\Delta ANKRD}$) or EV (LgBiT-EV) control and cotransfected or transduced with the small (Sm) BiT sequence fused to either p65 (SmBiT-p65) or EV (SmBiT-EV) into human embryonic kidney (HEK) 293T cells and *Trpv4* KO BMDMs (Fig. 5A). Transfection of LgBiT-TRPV4 and SmBiT-p65 plasmids was equal in HEK 293T cells (fig. S6). TRPV4-p65 interaction induced a reversible binding of BiT sequences, forming an active enzyme that catalyzed a luminescent reaction. LgBiT-EV and SmBiT-EV controls did not bind to each other in an appreciable manner (Fig. 5B). TRPV4^{FL} and the TRPV4$^{\Delta ANKRD}$ mutant supported similar amounts of Ca^{2+} influx when HEK 293T cells were stimulated with the TRPV4 agonist GSK1016790A (GSK), demonstrating that TRPV4 remains functional upon partial N-terminal deletion (fig. S7). Transfection of LgBiT-TRPV4$^{\Delta ANKRD}$ with SmBiT-p65 decreased luminescence >55% compared with LgBiT-TRPV4^{FL} and p65 (Fig. 5B). To validate the dependence of the TRPV4 ANKRD domain in macrophages, we transduced the LgBiT and SmBiT constructs into *Trpv4* KO BMDMs. Similarly, the TRPV4 ANKRD domain was essential for binding to p65

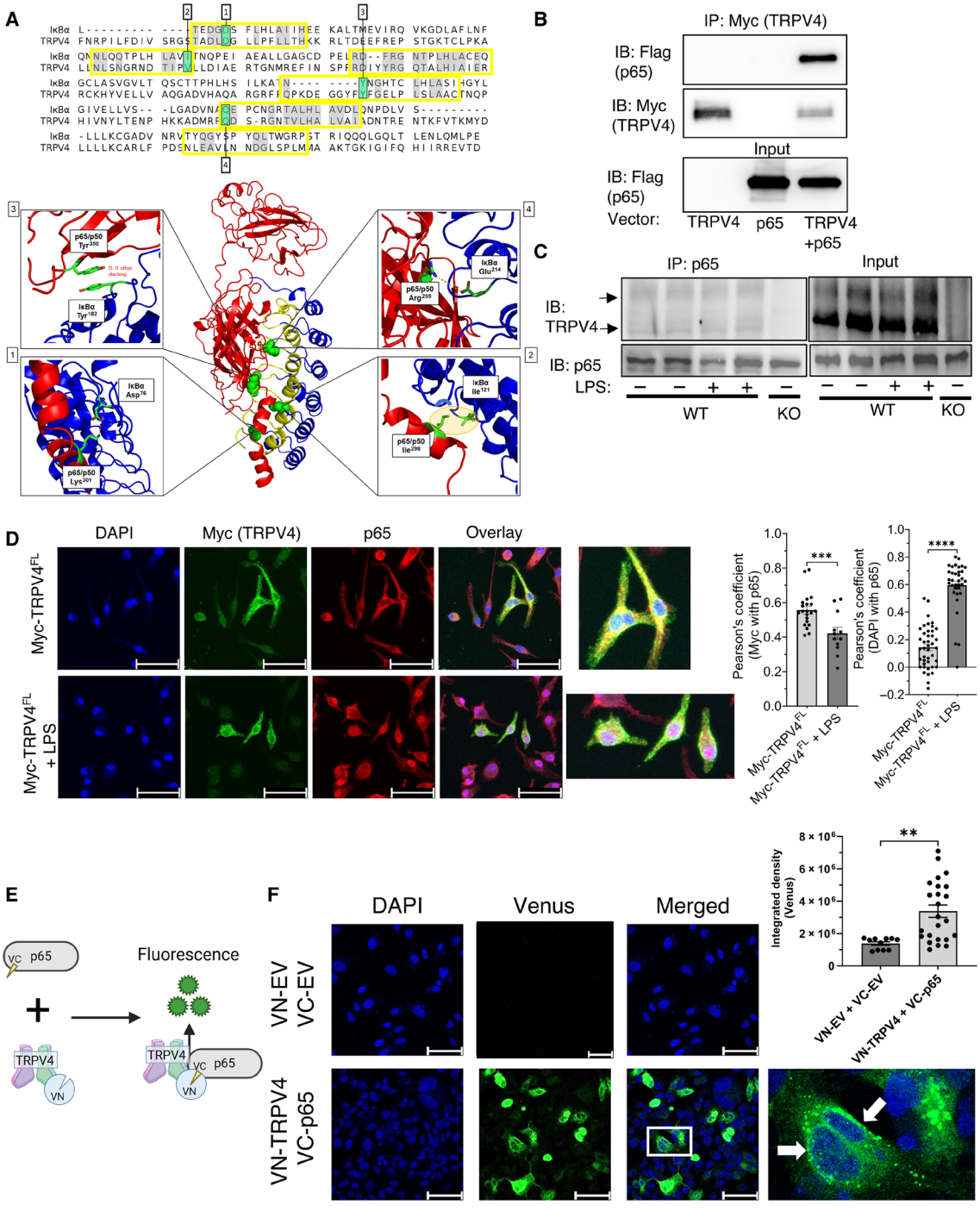

Fig. 4. The ANKRD of TRPV4 mediates binding to p65 under basal and LPS conditions. (**A**) Sequence alignment of the p65-interacting region of human IκBα and the N-terminal domain of human TRPV4 and structural mapping of conserved residues onto the published structure of IκBα (blue) and the NF-κB p65/p5 heterodimer (red) (PDB: 1NFI). Sequence similarity is noted with gray and green shading. Residues shown in green within the interacting interface (yellow boxes and yellow helices) were selected for structural mapping using the CLC Genomics Workbench (Qiagen). (**B**) Myc was immunoprecipitated (IP) from HEK 293T cells overexpressing Myc-tagged FL TRPV4, Flag-tagged p65, or both and immunoblotted (IB) for Flag and Myc. Input blot shows cell extracts without immunoprecipitation. $n = 3$ biological replicates per group. (**C**) p65 was immunoprecipitated from WT and *Trpv4* KO BMDMs ± LPS (100 ng/ml, 1 hour) and immunoblotted for p65 and TRPV4. $n = 3$ biological replicates per group. (**D**) *Trpv4* KO BMDMs, transduced with lentivirus encoding either EV or Myc-tagged TRPV4 FL, were treated ± LPS (100 ng/ml, 1 hour) and stained for Myc and p65. Nuclei were stained with DAPI. Scale bars, 50 μm. Rightmost images are magnified views from the overlays. Colocalization of p65 with Myc (yellow; >150 cells were analyzed per experiment on average) and DAPI (pink; 40 to 50 cells were analyzed) was quantified by Pearson's coefficient. $n = 3$ biological replicates per group. $^{***}P \leq 0.001$; $^{****}P \leq 0.0001$, by Student's *t* test. (**E**) Schematic demonstrating the BiFC method used to test interaction between TRPV4 and p65. (**F**) HeLa cells cotransduced with plasmids encoding either EV VN and VC constructs or VN-tagged TRPV4 and VC-tagged p65. Green fluorescence indicates interaction between the VN and VC tags. The white box indicates the area shown in higher magnification. Scale bars, 75 μm. Whole-image Venus intensity was quantified. $n = 3$ biological replicates per group (>500 cells were analyzed per experiment on average). $^{**}P \leq 0.01$, by Student's *t* test.

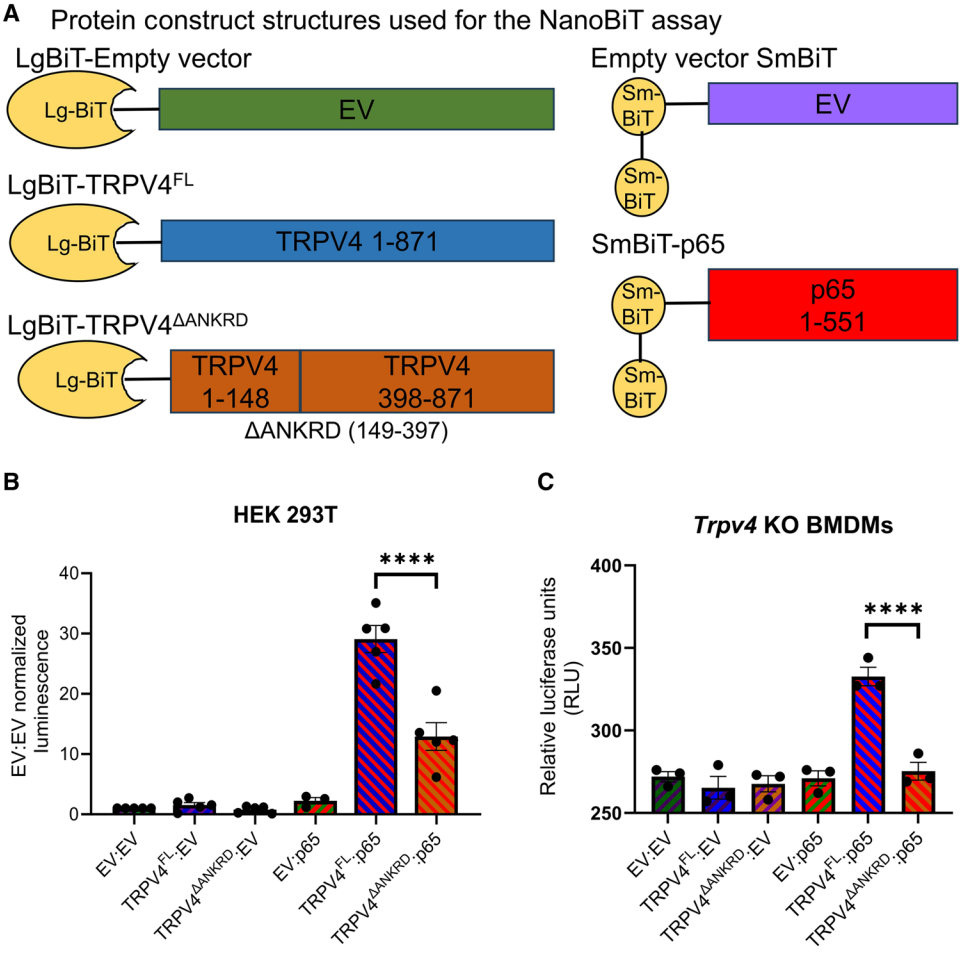

Fig. 5. The ANKRD is essential for TRPV4 binding to p65. (**A**) Schematic of NanoBiT constructs with LargeBiT (Lg-BiT) EV, TRPV4 FL, and TRPV4 ANKRD-deleted (ΔANKRD) and SmallBiT (Sm-BiT) EV and p65 FL. (**B** and **C**) Quantification of luminescence in HEK 293T cells (B) and *Trpv4* KO BMDMs (C) transfected or transduced, respectively, with the indicated plasmids. Luminescence is expressed as relative to that in cells expressing LgBiT-EV and SmBiT-EV (EV:EV). Immunoblotting to demonstrate transfection efficiency is shown in the Supplementary Materials (fig. S6). $n = 5$ biological replicates (HEK 293T cells) and 3 biological replicates (BMDMs) per group. ****$P \leq 0.0001$, by Student's *t* test.

(Fig. 5C). These data demonstrated in multiple systems, including primary macrophages, that the TRPV4 ANKRD was essential for TRPV4-p65 binding.

TRPV4 translocates from the ER to the plasma membrane upon LPS stimulation in macrophages

The locations of TRPV4 and p65 within the cell are important for a variety of TRPV4's functions (*29, 35, 36*). We previously showed that LPS increases TRPV4-dependent Ca^{2+} influx in a stiffness-dependent manner, suggesting its translocation to the plasma membrane (*23*). Because TRPV4 is primarily localized to the ER, we examined the location at which TRPV4 interacts with p65 upon TLR activation. To determine the intracellular location of TRPV4 in the basal state, the cellular ER and cytoplasm were fractionated from BMDMs from WT and *Trpv4* KO mice. TRPV4 protein was detected mainly in the ER fraction in WT BMDMs when TRPV4 protein abundance was normalized to that of the ER protein calnexin (Fig. 6A). Specifically, the calnexin-normalized concentration of TRPV4 was decreased by 50% after 1 hour of LPS stimulation, and that decrease persisted at 3 hours, indicating a relative decrease in TRPV4 abundance in the ER membrane after LPS treatment (Fig. 6A). To further validate the translocation of TRPV4 from the ER membrane after LPS treatment, immunofluorescence staining of the ER with calnexin was performed both in *Trpv4* KO BMDMs transduced with a Myc-$TRPV4^{FL}$ LV (Fig. 6B) and RAW267.4 macrophages transfected with a green fluorescent protein (GFP)–TRPV4 plasmid (fig. S8). The colocalization of TRPV4 and calnexin decreased by 50% upon LPS treatment as assessed by a reduction in Pearson's coefficient between $TRPV4^{FL}$ and calnexin, compared with untreated BMDMs and RAW267.4 cells, thereby confirming by an independent method in primary cells and a macrophage cell line that LPS induces a fraction of TRPV4 to translocate from the ER membrane. TRPV4 translocates to the plasma membrane to regulate functions such as Ca^{2+} influx upon stimulation with cytokines like transforming growth factor–β (TGF-β) in fibroblasts (*35, 37*). Upon LPS treatment, TRPV4 translocated to the plasma membrane, increasing its abundance in the plasma membrane by 150% within 1 hour of LPS treatment (Fig. 6C). Collectively, these data revealed that, in the basal state, TRPV4 resides predominately in the macrophage ER membrane, with its N-terminal ANKRD interacting in an inhibitory manner with cytoplasmic p65. Upon LPS stimulation, TRPV4 translocated to the plasma membrane, allowing release of p65 from the inhibitory complex for entry into the nucleus, where it induced the transcription of genes encoding proinflammatory cytokines (Fig. 7).

DISCUSSION

It has long been appreciated that the NF-κB family of transcription factors are master regulators of inflammation (*16*). A complex network of inducible kinases, cofactors, and inhibitors is needed to orchestrate proinflammatory cytokine secretion, facilitating a return to immune homeostasis quickly to prevent collateral tissue damage (*29*). Although many regulators of the NF-κB pathway have been identified, the contribution of the chemical and mechanical properties of the tissue microenvironment remains to be fully investigated. The present study identified a mechanosensitive cation channel, TRPV4, as a key regulator of the NF-κB pathway and its regulation of gene expression in lung macrophages. We substantiated these findings using complementary techniques in a mouse model and in primary mouse macrophages and cell lines to show that TRPV4 binding to p65 contributes to the suppression proinflammatory gene expression in lung macrophages during *P. aeruginosa* infection (Fig. 7).

Using complementary biochemical, colocalization, and functional methods, we showed that TRPV4 reduced NF-κB pathway activation

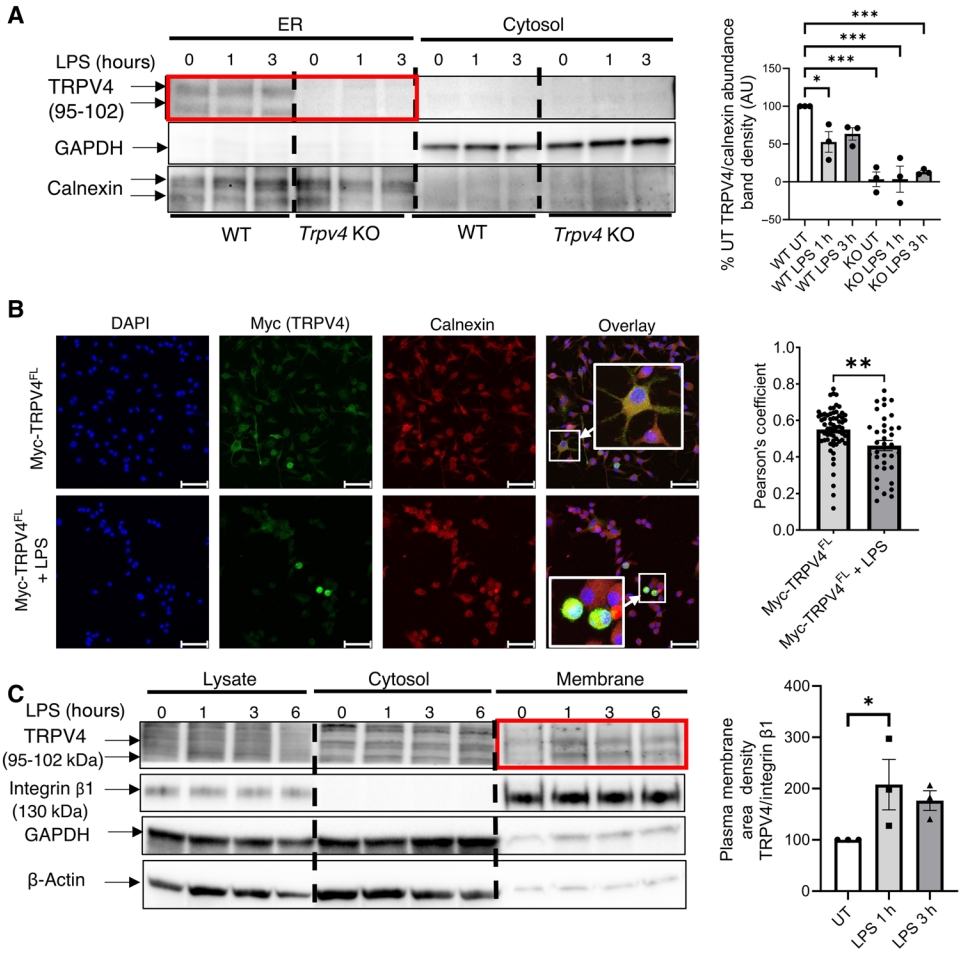

Fig. 6. TRPV4 resides in the ER under basal conditions and translocates to the plasma membrane after LPS stimulation. (**A**) WT and *Trpv4* KO BMDMs were treated with LPS for the indicated amounts of time. Cytosolic and ER fractions of the cells were immunoblotted for TRPV4, the ER marker calnexin, and the cytosolic protein GAPDH. The protein abundance of TRPV4 in the ER fraction (red box) was quantified and normalized to calnexin. $n = 3$ biological replicates per group. $^{*}P \leq 0.05$; $^{***}P \leq 0.001$ by one-way ANOVA with Šidák's MCT. AU, arbitrary units. (**B**) *Trpv4* KO BMDMs were transduced with Myc-tagged TRPV4^{FL}, stimulated with LPS (1 hour), and stained for Myc and the ER protein calnexin. Nuclei were stained with DAPI. Colocalization between Myc-TRPV4^{FL} and calnexin was quantified by Pearson's coefficient. Data points represent scores of Myc^{+} individual cells from combined experiments. Scale bars, 50 μm. $n = 3$ biological replicates per group (10 to 40 cells analyzed per replicate). $^{**}P \leq 0.01$, by Student's *t* test. (**C**) BMDMs from WT mice were treated with LPS for the indicated amounts of time, and whole-cell lysates, cytosolic, and plasma membrane fractions were immunoblotted for TRPV4, the plasma membrane protein integrin β1, and the cytosolic protein GAPDH. TRPV4 in the plasma membrane fractions (red box) was quantified relative to the amount in cells at time 0. $n = 3$ biological replicates per group, $^{*}P \leq 0.05$ by one-way ANOVA with Fisher's least significant difference (LSD).

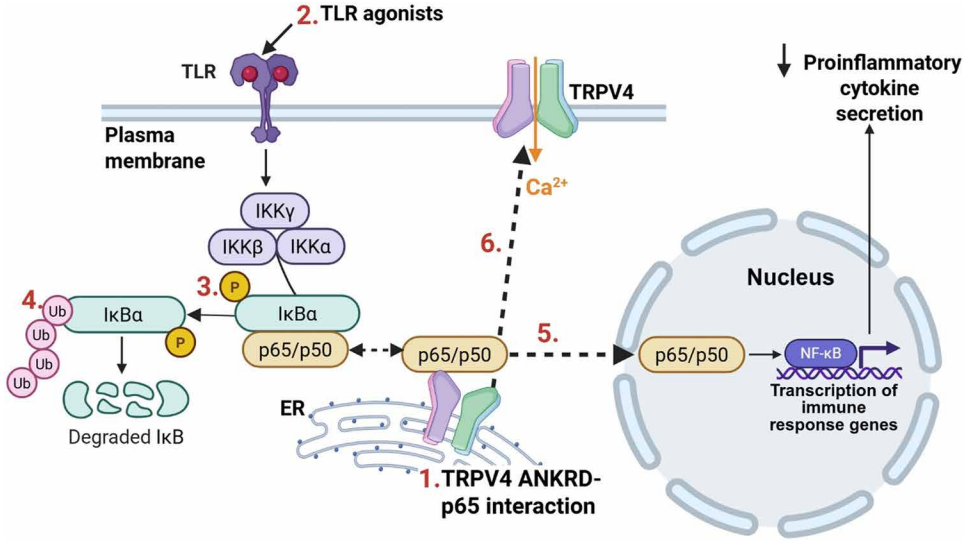

Fig. 7. Model for TRPV4-mediated inhibition of p65-dependent expression of proinflammatory transcripts. Under basal conditions (1), the TRPV4 N-terminal tail ANKRD interacts with the NF-κB subunit p65, possibly exchanging with IκBα on the ER membrane, limiting the nuclear translocation of p65. Upon TLR agonism (2), IKKβ phosphorylates IκBα (3), which leads to IκBα dissociation and proteasomal degradation (4). A fraction of p65 dissociates from TRPV4 in the ER and translocates to the nucleus, where it promotes the expression of proinflammatory genes (5), whereas the dissociated TRPV4 fraction translocates to the plasma membrane (6). Created with BioRender.

through the binding of its ANKRD to p65, which limited IκBα degradation. Our data supported that there are both p65-bound and p65-unbound fractions of TRPV4 under basal conditions and that LPS stimulates the dissociation of TRPV4-p65, thereby freeing TRPV4 and p65 to translocate to the plasma membrane and nucleus, respectively. Upon LPS stimulation, proinflammatory gene transcription reflected the action of the increased p65-dissociated fraction of TRPV4 (Fig. 7). The residual p65-bound TRPV4 fraction caused a net reduction of p65-dependent proinflammatory gene transcription (Fig. 7). This study identified the mechanosensitive Ca^{2+} channel

TRPV4 as a negative regulator of NF-κB complex function, thereby restoring homeostasis and dampening inflammation.

The pulmonary macrophage response during acute infection is coordinated between resident (TR-AMs) and recruited (Mo-AMs) macrophages (*9*). Resident alveolar macrophages are a first line of defense against pathogens and escalate the inflammatory response by activating and recruiting other immune cells (*38*). Recruited Mo-AMs secrete inflammatory cytokines and reactive oxygen species to control infection, but excessive or prolonged recruitment can cause collateral lung damage (*39*). Others have implicated a subset of monocyte-derived lung cells to have matrix-specific gene expression, which supports our findings that a mechanosensor (TRPV4) could drive lung macrophage function (*40*). By specifically targeting TRPV4 in $Cd11c^{+}$ alveolar macrophages in vivo (Fig. 1), we demonstrated that TRPV4 dampens the lung injury response, as evidenced by increased abundance of acute-phase chemoattractants and activators in the BALF from alveolar macrophage–specific *Trpv4* KO mice ($Cd11c$Cre:$Trpv4^{fl/fl}$). Specifically, upon lung digestion, the recruited Mo-AMs (Siglec-F^{-}) were the key population expressing NF-κB/p65-dependent proinflammatory cytokines (IL-1β and CCL2). These data are further supported by the increased NF-κB–dependent transcripts (*Ccl4*, *Ccl7*, and *Ccl2*) in a cluster of BMDMs expressing IL-1β and CXCL2 by single-cell RNA sequencing (scRNA-seq). These data are consistent with our prior work that TRPV4 in alveolar macrophages drives bacterial clearance and cytokine secretion in vitro (*24*). On the basis of the changes in the neutrophil chemoattractants in vitro and in vivo, we show that macrophage TRPV4 dampens neutrophil recruitment and consequently decreases lung inflammation after infection.

Prior works highlighted that TRPV4 in alveolar macrophages and BMDMs is necessary to limit proinflammatory cytokine secretion and decrease lung injury in vitro and in vivo (*23*, *24*). Here, we sought to uncover the mechanism by which TRPV4 inhibits inflammation. Macrophages exhibit dynamic changes in cell shape upon matrix contact and upon navigating channels between the interstitial and alveolar spaces within the lung (*41, 42*). Changes in cell shape alter macrophage polarization and NF-κB activation (*17, 37, 41–43*). Increases in extracellular matrix stiffness have also been directly linked to NF-κB activation (phosphorylation of p65 and degradation of IκB) in multiple cell types and under pathogenic conditions that require cells to migrate and frequently divide, such as cancer (*43, 44*). In addition, in multiple cancer cell lines, NF-κB activation, as measured by p65 nuclear translocation, correlates with cell physical characteristics such as cell area, spreading, polarity, and protrusions (*44*). Identifying how the macrophage recognizes a specific site of injury or maintains tissue integrity during health is an essential part of controlling inflammation and reversing ongoing lung tissue injury. Although previous works identified TRPV4 as the key mechanosensor on macrophages that drive lung inflammation (*23*, *24*), its intracellular signaling pathway in these cells has not been explored.

The key regulatory step of the NF-κB pathway starts with the IκB kinase complex (IKK) acting on the IκBs (IκBα, IκBβ, and IκBγ), which leads to ubiquitylation and degradation of IκBs and translocation of the transcription factors (p65, p50, and p52) to the nucleus (Fig. 7) (*45, 46*). However, contextual stimuli may specifically dictate IκB stabilization, phosphorylation, and degradation. TRPV4 directly binds to other proteins and kinases to signal intracellularly through its cytoplasmic tail (*20*, *30*), and our work reveals that the ANKRD of TRPV4, which was not required for TRPV4 to mediate Ca^{2+} influx, bound to and inhibited p65 and exhibits several characteristics similar to the homologous ANKRD of the IκB family. The TRPV4 ANKRD-p65 interaction localized to the ER membrane (*47*). Our data point to the concept that loss of TRPV4 on the ER membrane allows for priming of the macrophages in the basal state and then, upon LPS stimulation, leads to faster degradation of IκBα (Fig. 3C). However, there are still some unanswered questions. It remains possible that TRPV4's N-terminal ANKRD acts as a higher-order complex sequestering the NF-κB signaling kinase complex in the perinuclear cytosolic region and that posttranslational modification (for example, phosphorylation or acetylation) occurs upon TLR agonism and dissociates the TRPV4-NF-κB/p65 complex (*48–50*). The precise molecular interaction among TRPV4 and the NF-κB complex in vivo in the setting of chronic inflammation is a topic for future investigation.

It remains teleologically uncertain why a mechanosensitive cation channel would biologically inhibit NF-κB action in the basal state. However, the TRPV4-p65 interaction may occur as a means to dampen the early acute inflammatory response and enhance subsequent wound healing or scar formation upon the cell sensing a stiffened extracellular matrix (*23*, *24*). These signals and the nature of the TRPV4-p65 interaction under these conditions have yet to be identified. Further work to understand this complexity and the role of calcium may allow for targeting and altering innate immune signals in response to infection or injury.

Notwithstanding the need for further studies, our work advances the understanding of the potential contribution of the mechanosensors in the stiffened microenvironment to the innate immune response in the lung, yet there are some limitations. Most of our in vitro systems require overexpression techniques, a consequence of limited available reagents. We also needed to validate the location of TRPV4 and p65 using immunofluorescence that is inherently less quantitative but confirmed the biochemical assays. In addition, activation of the NF-κB signaling cascade occurs rapidly and with overlapping activation signals; thus, identification of specific activation partners is difficult to achieve. However, we validated key readouts such as p65 and TRPV4 coimmunoprecipitation endogenously and NanoBiT binding in primary macrophages. Also, we have shown the macrophage TRPV4 response to *P. aeruginosa*, which activates multiple TLRs, in vivo. Given that this work was limited to in vitro studies to examine the mechanism, we will investigate in vivo biology using TRPV4 mutants deficient in p65 binding in future studies to determine the implication of TRPV4-mediated regulation of the NF-κB pathway on lung injury.

In conclusion, inflammation in the lung is a complex process that depends on the NF-κB pathway. Innate immune cells such as macrophages are essential to calibrate the inflammatory response to resolve injury and begin repair in the setting of bacterial pneumonia. Our data suggest that TRPV4 is a mechanosensitive channel that binds to the NF-κB complex to act as an inhibitor, similar to that of IκBα, regulating proinflammatory cytokine gene expression. Regulation of proinflammatory pathways by microenvironmental signals is important to the pathogenesis of many inflammatory diseases outside of bacterial pneumonia–associated ARDS, indicating the broad applicability of this work.

MATERIALS AND METHODS

Antibodies and reagents

Primary antibodies to extracellular and intracellular TRPV4 (Alomone Labs, Jerusalem Israel; Cell Signaling), glyceraldehyde-3-phosphate dehydrogenase (GAPDH; Fitzgerald Industries International, Acton,

MA), total NF-κB/p65 (Cell Signaling), IκBα (Santa Cruz Biotechnology), integrin β1 (BD Biosciences), β-actin (Abcam), and GSK (Sigma-Aldrich) were obtained from commercial vendors. Pam3CSK4, Poly I:C, CpGDNA, Myc, and calnexin were obtained from Cell Signaling. *Escherichia coli* LPS 0111:B4 was obtained from Sigma-Aldrich.

Cell culture, transfection, immunoblotting, plasma membrane and cytoplasmic isolation, and cytokine measurement

All animal protocols were performed as approved by the Cleveland Clinic Institutional Animal Care and Use Committee (IACUC) under protocol no. 2624. Primary murine BMDMs were harvested from 8- to 12-week-old C57BL/6 WT, TRPV4-null (*Trpv4* KO), or B6(SJL)-Rela$^{tm2.1}$Alex/J mice. BMDMs were differentiated in recombinant macrophage colony-stimulating factor (M-CSF) (50 ng/ml; R&D Systems) as previously published (*23*, *24*). Cells were treated with Pam3CSK4 (100 ng/ml, 1 hour), LPS (0.1 to 10 μg/ml, 6 to 24 hours), poly I:C (10 μg/ml, 1 to 3 hours), or CpG DNA (5 μg/ml, 1 to 3 hours). HeLa cells [American Type Culture Collection (ATCC), CCL-2], HEK 293T (ATCC, CRL-3216), and RAW267.4 (ATCC) were cultured per standard culture conditions as previously published (*23*). TRPV4 overexpression was achieved by transfecting 293T and HeLa cells with the Myc-TRPV4 plasmid construct, as previously published (*35, 51*). RAW267.4 cells were transfected with the GFP-TRPV4 plasmid construct, as previously published (*35, 51*). *Trpv4* KO BMDMs were transduced with Myc-EV or Myc-TRPV4^{FL} lentiviral constructs (VectorBuilder) for colocalization studies. p65 expression was downregulated by transfecting BMDMs with mouse p65-specific siRNA duplexes or scrambled siRNA controls (Dharmacon) using electroporation, as previously published (*23*). Immunoblotting was performed for selected proteins as previously published (*23*, *24*). To measure the time course changing of IκBα and nuclear p65, BMDMs from WT and KO mice were differentiated and treated with HC-067047 (MedChemExpress, HY-100208) and/or LPS (50 to 100 ng/ml) for the indicated time. Cell extracts were immunoblotted with the indicated antibodies. IκBα and nuclear p65 protein were quantified and normalized to GAPDH or Lamin B levels. ER and cytosol fractionation was performed via published protocols, and immunoblots were performed; fractions were normalized to GAPDH and calnexin (*35, 52, 53*). Enzyme-linked immunosorbent assays (ELISAs; IL-1β from R&D systems) were run on conditioned media from WT BMDMs with/without LPS and *Trpv4* KO BMDMs as previously published (*23*, *24*).

P. aeruginosa mouse model of acute pneumonia

P. aeruginosa PAM57-15 (mucoid clinical isolate) was used at a sublethal dose of 10^5 to 10^6, and sterile culture was instilled intranasally in female alveolar macrophage–specific Trpv4 KO mice (*Cd11c*Cre × *Trpv4*$^{fl/fl}$) and age-matched *Trpv4*$^{fl/fl}$ mice (Case Western Reserve). Mice were anesthetized with aerosol isoflurane inhalation, and *P. aeruginosa* were instilled intranasally in a volume of 40 μl to allow infection to reach deep airspaces (*54*). Total bacterial concentration instilled was measured before instillation [colony-forming units per millilter (CFU/ml)] as previously published (*24*). Treatment course was monitored as described previously (*24*). Two days after bacterial installation, BAL and BALF were obtained for total cell count, differential, and cytokine measurement using LEGENDplex, Mouse Proinflammatory Chemokine Panel V02 (BioLegend, catalog no. 741295) per the manufacturer's instructions.

The original strain of *Trpv4*$^{fl/fl}$ was obtained from the Case Transgenic and Targeting Facility at Case Western Reserve. Embyonic stem cells were obtained from the Mutant Mouse Research & Research Center (MMRRC) and implanted to obtain chimeric mice. *Cd11c*Cre (the Jackson Laboratory, strain no. 008068) mice in which Cre recombinase is knocked in to C57BL/6J mice at a location separate from endogenous Cd11c. *Cd11c*Cre × *Trpv4*$^{fl/fl}$ mice were generated by crossing the two strains. Genotyping was completed using TransnetYX services, and mice either hemizygous or heterozygous for *Cd11c*Cre and homozygous for *Trpv4*$^{fl/fl}$ were selected for experimentation. In our laboratory, we have further backcrossed to C57BL/6 animals to maintain the background. Mice for experimentation were between the ages of 8 and 12 weeks.

Flow cytometry

Animals infected with *P. aeruginosa* were euthanized, and lungs were perfused with cold phosphate-buffered saline (PBS). Lung tissue was digested by mincing and incubating with collagenase I (1 mg/ml; catalog no. LS004196; Worthington Biochemical), DNase I (5 mg/ml; D4263, Sigma-Aldrich), and RBC lysis buffer (catalog no. 50-112-9743, Thermo Fisher Scientific). Single-cell suspension was counted manually, and cell differential was determined by cytospin. Five million cells per condition were preincubated with Fc block (catalog no. 553141, BD Biosciences) and stained with CD45 (30-F11) BV785 (1:500; BioLegend), F4/80 (BM8) PE-Cy5 (1:500; BioLegend), and Siglec-F(S17007L) PE-Dazzle594 (1:500; BioLegend). Cells were then incubated with Zombie Aqua Fixable Viability (BioLegend) to exclude dead cells according to the manufacturer's instructions. Using the FIX & PERM Cell Fixation Kit (Life Technologies), cells were fixed and permeabilized. Following this, cells were incubated with IL-1β (NJTEN3) PE (1:500; Invitrogen) and CCL2(2H5) FITC (1:500; Invitrogen). All antibodies were titrated to determine optimal staining concentrations for our specific application. Staining was performed in cluster tubes of 250-μl volume on ice incubated for 30 min. Samples were run on a FACSymphony A1 (BD Biosciences) flow cytometer with standard configuration with 50,000 to 100,000 events acquired. Data were analyzed using FlowJo10 software (Tree Star). Dead cells and cell debris were excluded before gating for macrophage markers.

10X Genomics single-cell sequencing

BMDMs from three individual WT and three individual *Trpv4* KO mice ± LPS ($n = 12$ total samples) differentiated as above were analyzed using 10X Genomic Sequencing. CellRanger (v3.1.0) was used for alignment of raw FASTQs to the mm10 reference genome. Downstream analyses were performed using the Seurat package (v4) in R (v4.2). Raw counts were used from a filtered feature matrix for each sample. Cells were filtered for >250 nonzero gene counts, >1000 unique transcripts, <40,000 unique transcripts, and <10% mitochondrial transcripts. Integration and clustering were performed on a per sample basis. A total of 3000 features were used for integration. Following principal component analysis Uniform Manifold Approximation and Projections (UMAPs) were visualized with 40 dimensions. Differential marker gene expression was found using "FindAllMarkers" both overall and within each cluster, which uses a Wilcoxon rank sum test. Pathway analyses were performed on these gene lists using gprofiler.

NF-κB response element reporter assay and mVenus-RELA (p65) reporter assay

Plasmid containing the NF-κB response element was synthesized by Integrated DNA Technologies (Coralville, IA) and subcloned in

the pGL3-basic vector (Promega, Madison, WI). HeLa cells (ATCC, CCL-2) were grown in Dulbecco's modified Eagle's medium (DMEM) containing 10% fetal bovine serum (FBS) and penicillin/streptomycin (100 U/ml) and were transfected at 60% confluence with the TRPV4 and pGL3-basic plasmid construct using Lipofectamine 3000 (Life Technologies) according to the manufacturer's protocol. The pRL-TK Renilla plasmid (Promega) was used as an internal control. The next day, cells were washed with warm PBS and then incubated in DMEM growth medium containing the indicated reagents as described in the figures. After overnight incubation, cells were harvested, and luciferase activities were determined by a Dual-Luciferase Reporter Assay kit (Promega; Millipore no. SCT152).

B6(SJL)-Rela$^{tm2.1}$Alex/J mice were purchased from the Jackson Laboratory (strain no. 038987), and BMDMs were acquired as described above. TRPV4 expression was down-regulated by transfecting BMDMs with mouse *Trpv4*-specific siRNA duplexes or scrambled siRNA controls (Origene) using electroporation, as previously published (*23*). Cells were treated for 1 hour with LPS (1 μg/ml) before being scraped and put through a 35-μm filter. Cells were incubated with LIVE/DEAD Fixable Aqua Dead Cell Stain (1:1000; Invitrogen). Samples were run on a FACSymphony A1 (BD Biosciences) flow cytometer with standard configuration with 5000 to 10,000 events acquired. Data were analyzed using FlowJo10 software (Tree Star). Dead cells and cell debris were excluded before analyzing the mean fluorescence intensity (MFI) of mVenus fluorescence.

Real-time quantitative PCR

Total RNA was extracted using TRIzol reagent (Thermo Fisher Scientific Inc., Waltham, MA) or RNeasy Mini Kit from Qiagen (Germantown, MD) following the manufacturers' protocols. cDNA was generated from 1 μg of total RNA using a High-Capacity RNA-to-cDNA kit (Thermo Fisher Scientific Inc.). Real-time quantitative polymerase chain reaction (qPCR) analysis was performed using synthesized primers (detailed below) and measured by the SYBR Green method. mRNA values were normalized to *Gapdh* mRNA. Gene expression was calculated using the $2^{-\Delta\Delta CT}$ method and reported relative to WT control cells for the indicated agonist.

Gapdh_F: AGGTCGGTGTGAACGGATTTG; Gapdh_R: TGTAGACCATGTAGTTGAGGTCA; Cxcl1_F: CTGGGATTCACCTCAAGAACATC; Cxcl1_R: CAGGGTCAAGGCAAGCCTC; Il1b_F: GCAACTGTTCCTGAACTCAACT; Il1b_R: ATCTTTTGGGGTCCGTCAACT.

Construct generation, cloning, and NanoBiT experiment

The NanoBiT Protein:Protein Interaction (PPI) system (Promega) was used as a luciferase-based assay to measure TRPV4 and p65 protein interaction. hRELA/p65, hTRPV4^{FL}, and hTRPV4$^{\Delta ANKRD}$ with cDNA fragment were synthesized and purchased (Azenta). hRELA/p65, hTRPV4^{FL}, and hTRPV4$^{\Delta ANKRD}$ constructs were fused with Large BiT (pBiT2.1[TK/LgBiT], LgBiT) (hTRPV4^{FL} and hTRPV4$^{\Delta ANKRD}$) and Small BiT (pBiT2.1-N [TK/SmBiT], Sm-BiT) (hRELA/p65) using the Clone Express II One Step Cloning Kit (Vazyme) and vectors that contain a cytomegalovirus (CMV) promotor for mammalian expression.

HEK 293T cells were seeded at 4×10^4 cells per well in a 96-well plate. Following overnight incubation, cells were transfected using Lipofectamine 3000 (Invitrogen). Cells were transfected with both an Lg-BiT (EV, hTRPV4^{FL}, and hTRPV4$^{\Delta ANKRD}$) and an Sm-BiT (EV and hRELA/p65) construct with two technical replicates per condition. Transfected cells were incubated for 16 hours to allow for expression of fusion proteins. The Nano-Glo Vivazine substrate was added to each condition and incubated for 1 hour in the dark to allow for stable signal. Luminescence was read on a SpectraMax ID5 plate reader (Molecular Devices) every 5 min for 2 hours.

Trpv4 KO BMDMs were seeded at 4×10^4 cells per well in a 96-well plate. Following overnight incubation, cells were transduced with LV packed in house using a second-generation LV system packaged in HEK 293T cells. The packaged virus was pooled for 3 days and then filtered before being placed on the *Trpv4* KO BMDMs and spun for 1 hour at 951*g*. Following 16 hours of incubation, the LV was removed and cells were supplemented with complete medium. Cells were transduced with both an Lg-BiT (EV, hTRPV4^{FL}, and hTRPV4$^{\Delta ANKRD}$) and an Sm-BiT (EV and hRELA/p65) construct with two technical replicates per condition. Transduced cells were incubated for 48 hours following virus removal to allow for expression of fusion proteins. The Nano-Glo Vivazine substrate was added to each condition and incubated for 1 hour in the dark to allow for stable signal. Luminescence was read on a SpectraMax ID5 plate reader (Molecular Devices) every 5 min for 2 hours.

Interaction of hRELA and hTRPV4 was detected with a rise in luminescence, indicating interaction of the Lg-BiT and Sm-BiT forming a productive enzyme. The baseline signal can be observed in control samples indicating free Lg-BiT and Sm-BiT diffusion-limited interactions. Data were normalized to Lg-BiT and Sm-BiT EVs control condition at the 1-hour and 30-min time point corresponding to peak enzyme activity.

Measurement of intracellular calcium

The calcium response to TRPV4 agonist (GSK) was analyzed using fluorescent Calcium 5 dye (Molecular Devices)–treated cells in a microplate reader as previously published (*51*). Cytosolic calcium increases (Ca^{2+} influx) are presented as RFU above EV.

Coimmunoprecipitation

To assess the interaction between TRPV4 and proteins in the NF-κβ pathway, HeLa and 293T cells were transfected with the N-terminal, Myc-tagged TRPV4^{FL} plasmid or Flag-tagged p65 plasmid for 24 hours. Cell lysates were prepared as described above. Aliquots containing equal protein were reacted with mouse ChromoTek Myc-Trap Agarose beads for 1 hour at 4°C, followed by washing four times antigen-bead complexes with tris-buffered saline with 0.05% Tween-20 (TBST) at 4°C. Immunoadsorbed proteins and total cell lysates were separated on 8% SDS–polyacrylamide gel electrophoresis (PAGE) gels and immunoblotted with antibodies against Myc or p65 (CST; 1:5000). When assessing the interaction at the endogenous level, BMDMs' extracts were immunoprecipitated with p65 antibody (CST; 1:200) overnight and reacted with protein A/G agarose beads.

Immunofluorescence

For Myc constructs, *Trpv4* KO BMDMs were plated with standard tissue conditions on chamber slides (ibidi no. 80841) and transduced with Myc-TRPV4^{FL} or EV LV for 6 hours. Cells were grown for 72 hours and then treated ± LPS for 1 hour (100 ng/ml). Likewise, RAW267.4 cells were transfected with the GFP-TRPV4 construct or EV and treated ± LPS. For bimolecular fluorescence complementation (BiFC), HeLa cells were transfected with VN-EV + VC-EV or VN-tagged TRPV4 and VC-tagged p65. After treatment, cells were

fixed with 4% paraformaldehyde (PFA). For staining, cells were permeabilized with 0.03% Triton X-100 and blocked with 5% normal goat serum. Cells were stained overnight at 4°C with primary anti-p65 (1:500) or anti-calnexin antibody (1:200), followed by Alexa Fluor 568 secondary antibody (1:500, 1 hour at room temperature) in blocking solution. Slides were mounted with ProLong Gold Antifade with DAPI (Invitrogen, no. P36935). Images were acquired using a Leica SP8 inverted confocal microscope at 40× and 63× original magnification and processed with LAS X software. Pearson's coefficient was calculated by manually isolated fields using Volocity and ImageJ software.

Bimolecular fluorescence complementation

HeLa cells were plated on chamber slides (ibidi) with 10,000 cells per well and allowed to adhere for 6 hours. Cells were transfected using polyethyleneimine with combinations of VN-TRPV4 tag, VC-p65, and their corresponding EV controls. After transfections, cells were incubated for 24 hours to allow protein expression. Cells were fixed using 4% PFA in PBS for 20 min at 4°C. Slides were washed with PBS and coverslips mounted using ProLong Gold Antifade Mountant with DAPI and allowed to set overnight. Images were acquired using a Leica SP8 inverted confocal microscope at 40× and 63× original magnification and processed with LAS X software. A positive experiment has fluorescence corresponding to Venus excitation and emission under the VN-TRPV4:VC-p65 condition, as quantified by whole-image integrated intensity using ImageJ software.

Sequence alignment

Sequence alignment of the human IκBα and human TRPV4 N-terminal domain was generated using the CLC Genomics Workbench. Selected residues were annotated using Microsoft PowerPoint. Structures were visualized and figures prepared using the Pymol Molecular Visualization system using Protein Data Bank (PDB) entry 1NFI.

Statistical analysis

Statistical analysis between two groups was performed by an unpaired Student's *t* test. For multiple comparison between groups, statistical analysis was performed by one-way analysis of variance (ANOVA) with Bonferroni or Šidák's multiple-comparison test (MCT) or two-way ANOVA with Tukey's MCT to determine adjusted *P* values (Prism, GraphPad Software, La Jolla, CA). All graphs in this paper are displayed with error bars corresponding to SEM. In all cases, *P* values < 0.05 were considered statistically significant. Each figure panel contains information on statistical tests used and *P* values for which significance mark denotes.

Supplementary Materials

The PDF file includes:
Figs. S1 to S8

Other Supplementary Material for this manuscript includes the following:
MDAR Reproducibility Checklist

REFERENCES AND NOTES

1. J. A. Ramirez, T. L. Wiemken, P. Peyrani, F. W. Arnold, R. Kelley, W. A. Mattingly, R. Nakamatsu, S. Pena, B. E. Guinn, S. P. Furmanek, A. K. Persaud, A. Raghuram, F. Fernandez, L. Beavin, R. Bosson, R. Fernandez-Botran, R. Cavallazzi, J. Bordon, C. Valdivieso, J. Schulte, R. M. Carrico, University of Louisville Pneumonia Study Group, Adults hospitalized with pneumonia in the United States: Incidence, epidemiology, and mortality. *Clin. Infect. Dis.* **65**, 1806–1812 (2017).
2. T. T. Bauer, S. Ewig, A. C. Rodloff, E. E. Müller, Acute respiratory distress syndrome and pneumonia: A comprehensive review of clinical data. *Clin. Infect. Dis.* **43**, 748–756 (2006).
3. L. B. Ware, M. A. Matthay, The acute respiratory distress syndrome. *N. Engl. J. Med.* **342**, 1334–1349 (2000).
4. G. B. Toews, Cytokines and the lung. *Eur. Respir. J. Suppl.* **18**, 3s–17s (2001).
5. W. J. Branchett, C. M. Lloyd, Regulatory cytokine function in the respiratory tract. *Mucosal Immunol.* **12**, 589–600 (2019).
6. B. A. David, P. Kubes, Exploring the complex role of chemokines and chemoattractants in vivo on leukocyte dynamics. *Immunol. Rev.* **289**, 9–30 (2019).
7. T. R. Martin, C. W. Frevert, Innate immunity in the lungs. *Proc. Am. Thorac. Soc.* **2**, 403–411 (2005).
8. C. C. Bain, A. S. MacDonald, The impact of the lung environment on macrophage development, activation and function: Diversity in the face of adversity. *Mucosal Immunol.* **15**, 223–234 (2022).
9. F. Hou, K. Xiao, L. Tang, L. Xie, Diversity of macrophages in lung homeostasis and diseases. *Front. Immunol.* **12**, 753940 (2021).
10. F. Y. McWhorter, C. T. Davis, W. F. Liu, Physical and mechanical regulation of macrophage phenotype and function. *Cell. Mol. Life Sci.* **72**, 1303–1316 (2015).
11. X. Geeraerts, J. Fernández-Garcia, F. J. Hartmann, K. E. de Goede, L. Martens, Y. Elkrim, A. Debraekeleer, B. Stijlemans, A. Vandekeere, G. Rinaldi, R. de Rycke, M. Planque, D. Broekaert, E. Meinster, E. Clappaert, P. Bardet, A. Murgaski, C. Gysemans, F. A. Nana, Y. Saeys, S. C. Bendall, D. Laoui, J. van den Bossche, S. M. Fendt, J. A. van Ginderachter, Macrophages are metabolically heterogeneous within the tumor microenvironment. *Cell Rep.* **37**, 110171 (2021).
12. A. C. McQuattie-Pimentel, Z. Ren, N. Joshi, S. Watanabe, T. Stoeger, M. Chi, Z. Lu, L. Sichizya, R. P. Aillon, C.-I. Chen, S. Soberanes, Z. Chen, P. A. Reyfman, J. M. Walter, K. R. Anekalla, J. M. Davis, K. A. Helmin, C. E. Runyan, H. Abdala-Valencia, K. Nam, A. Y. Meliton, D. R. Winter, R. I. Morimoto, G. M. Mutlu, A. Bharat, H. Perlman, C. J. Gottardi, K. M. Ridge, N. S. Chandel, J. I. Sznajder, W. E. Balch, B. D. Singer, A. V. Misharin, G. R. S. Budinger, The lung microenvironment shapes a dysfunctional response of alveolar macrophages in aging. *J. Clin. Invest.* **131**, e140299 (2021).
13. T. Kawai, S. Akira, Signaling to NF-κB by Toll-like receptors. *Trends Mol. Med.* **13**, 460–469 (2007).
14. C. Weber, C. Müller, A. Podszuweit, C. Montino, J. Vollmer, A. Forsbach, Toll-like receptor (TLR) 3 immune modulation by unformulated small interfering RNA or DNA and the role of CD14 (in TLR-mediated effects). *Immunology* **136**, 64–77 (2012).
15. A. S. Sameer, S. Nissar, Toll-like receptors (TLRs): Structure, functions, signaling, and role of their polymorphisms in colorectal cancer susceptibility. *Biomed. Res. Int.* **2021**, 1157023 (2021).
16. K. Taniguchi, M. Karin, NF-κB, inflammation, immunity and cancer: Coming of age. *Nat. Rev. Immunol.* **18**, 309–324 (2018).
17. S. Ishihara, M. Yasuda, I. Harada, T. Mizutani, K. Kawabata, H. Haga, Substrate stiffness regulates temporary NF-κB activation via actomyosin contractions. *Exp. Cell Res.* **319**, 2916–2927 (2013).
18. K. T. Best, F. K. Lee, E. Knapp, H. A. Awad, A. E. Loiselle, Deletion of NFKB1 enhances canonical NF-κB signaling and increases macrophage and myofibroblast content during tendon healing. *Sci. Rep.* **9**, 10926 (2019).
19. A. Garcia-Elias, S. Mrkonjić, C. Pardo-Pastor, H. Inada, U. A. Hellmich, F. Rubio-Moscardó, C. Plata, R. Gaudet, R. Vicente, M. A. Valverde, Phosphatidylinositol-4,5-biphosphate-dependent rearrangement of TRPV4 cytosolic tails enables channel activation by physiological stimuli. *Proc. Natl. Acad. Sci. U.S.A.* **110**, 9553–9558 (2013).
20. N. Takahashi, S. Hamada-Nakahara, Y. Itoh, K. Takemura, A. Shimada, Y. Ueda, M. Kitamata, R. Matsuoka, K. Hanawa-Suetsugu, Y. Senju, M. X. Mori, S. Kiyonaka, D. Kohda, A. Kitao, Y. Mori, S. Suetsugu, TRPV4 channel activity is modulated by direct interaction of the ankyrin domain to $PI(4,5)P_2$. *Nat. Commun.* **5**, 4994 (2014).
21. J. P. White, M. Cibelli, L. Urban, B. Nilius, J. G. McGeown, I. Nagy, TRPV4: Molecular conductor of a diverse orchestra. *Physiol. Rev.* **96**, 911–973 (2016).
22. D. Jiang, R. Guo, R. Dai, S. Knoedler, J. Tao, H. G. Machens, Y. Rinkevich, The multifaceted functions of TRPV4 and calcium oscillations in tissue repair. *Int. J. Mol. Sci.* **25**, 1179 (2024).
23. R. G. Scheraga, S. Abraham, K. A. Niese, B. D. Southern, L. M. Grove, R. D. Hite, C. McDonald, T. A. Hamilton, M. A. Olman, TRPV4 mechanosensitive ion channel regulates lipopolysaccharide-stimulated macrophage phagocytosis. *J. Immunol.* **196**, 428–436 (2016).
24. R. G. Scheraga, S. Abraham, L. M. Grove, B. D. Southern, J. F. Crish, A. Perelas, C. McDonald, K. Asosingh, J. D. Hasday, M. A. Olman, TRPV4 protects the lung from bacterial pneumonia via MAPK molecular pathway switching. *J. Immunol.* **204**, 1310–1321 (2020).
25. W. J. Branchett, J. Cook, R. A. Oliver, N. Bruno, S. A. Walker, H. Stölting, M. Mack, A. O'Garra, S. Saglani, C. M. Lloyd, Airway macrophage-intrinsic TGF-β1 regulates pulmonary immunity during early-life allergen exposure. *J. Allergy Clin. Immunol.* **147**, 1892–1906 (2021).
26. E. M. Todd, J. Y. Zhou, T. P. Szasz, L. E. Deady, J. A. D'Angelo, M. D. Cheung, A. H. J. Kim, S. C. Morley, Alveolar macrophage development in mice requires L-plastin for cellular localization in alveoli. *Blood* **128**, 2785–2796 (2016).

27. H. L. Pahl, Activators and target genes of Rel/NF-κB transcription factors. *Oncogene* **18**, 6853–6866 (1999).
28. A. Adelaja, B. Taylor, K. M. Sheu, Y. Liu, S. Luecke, A. Hoffmann, Six distinct NFκB signaling codons convey discrete information to distinguish stimuli and enable appropriate macrophage responses. *Immunity* **54**, 916–930.e7 (2021).
29. T. Liu, L. Zhang, D. Joo, S.-C. Sun, NF-κB signaling in inflammation. *Signal Transduct. Target. Ther.* **2**, 17023 (2017).
30. S. Cao, A. Anishkin, N. S. Zinkevich, Y. Nishijima, A. Korishettar, Z. Wang, J. Fang, D. A. Wilcox, D. X. Zhang, Transient receptor potential vanilloid 4 (TRPV4) activation by arachidonic acid requires protein kinase A-mediated phosphorylation. *J. Biol. Chem.* **293**, 5307–5322 (2018).
31. H. Inada, E. Procko, M. Sotomayor, R. Gaudet, Structural and biochemical consequences of disease-causing mutations in the ankyrin repeat domain of the human TRPV4 channel. *Biochemistry* **51**, 6195–6206 (2012).
32. M. D. Jacobs, S. C. Harrison, Structure of an IκBα/NF-κB complex. *Cell* **95**, 749–758 (1998).
33. M. Tiwari, S. Mikuni, H. Muto, M. Kinjo, Determination of dissociation constant of the NFκB p50/p65 heterodimer using fluorescence cross-correlation spectroscopy in the living cell. *Biochem. Biophys. Res. Commun.* **436**, 430–435 (2013).
34. H. Du, P. Yin, X. Yang, L. Zhang, Q. Jin, G. Zhu, Enterovirus 71 2C protein inhibits NF-κB activation by binding to RelA. *Sci. Rep.* **5**, 14302 (2015).
35. L. M. Grove, M. L. Mohan, S. Abraham, R. G. Scheraga, B. D. Southern, J. F. Crish, S. V. Naga Prasad, M. A. Olman, Translocation of TRPV4-PI3Kγ complexes to the plasma membrane drives myofibroblast transdifferentiation. *Sci. Signal.* **12**, eaau1533 (2019).
36. M. Mamenko, O. L. Zaika, N. Boukelmoune, J. Berrout, R. G. O'Neil, O. Pochynyuk, Discrete control of TRPV4 channel function in the distal nephron by protein kinases A and C. *J. Biol. Chem.* **288**, 20306–20314 (2013).
37. S. Baratchi, P. Keov, W. G. Darby, A. Lai, K. Khoshmanesh, P. Thurgood, P. Vahidi, K. Ejendal, P. McIntyre, The TRPV4 agonist GSK1016790A regulates the membrane expression of TRPV4 channels. *Front. Pharmacol.* **10**, 6 (2019).
38. M. Kopf, C. Schneider, S. P. Nobs, The development and function of lung-resident macrophages and dendritic cells. *Nat. Immunol.* **16**, 36–44 (2015).
39. A. L. McCubbrey, L. Barthel, M. P. Mohning, E. F. Redente, K. J. Mould, S. M. Thomas, S. M. Leach, T. Danhorn, S. L. Gibbings, C. V. Jakubzick, P. M. Henson, W. J. Janssen, Deletion of c-FLIP from $CD11b^{hi}$ macrophages prevents development of bleomycin-induced lung fibrosis. *Am. J. Respir. Cell Mol. Biol.* **58**, 66–78 (2018).
40. K. J. Mould, C. M. Moore, S. A. McManus, A. L. McCubbrey, J. D. McClendon, C. L. Griesmer, P. M. Henson, W. J. Janssen, Airspace macrophages and monocytes exist in transcriptionally distinct subsets in healthy adults. *Am. J. Respir. Crit. Care Med.* **203**, 946–956 (2021).
41. F. Y. McWhorter, T. Wang, P. Nguyen, T. Chung, W. F. Liu, Modulation of macrophage phenotype by cell shape. *Proc. Natl. Acad. Sci. U.S.A.* **110**, 17253–17258 (2013).
42. R. Sridharan, A. R. Cameron, D. J. Kelly, C. J. Kearney, F. J. O'Brien, Biomaterial based modulation of macrophage polarization: A review and suggested design principles. *Mater. Today* **18**, 313–325 (2015).
43. M. Chen, Y. Zhang, P. Zhou, X. Liu, H. Zhao, X. Zhou, Q. Gu, B. Li, X. Zhu, Q. Shi, Substrate stiffness modulates bone marrow-derived macrophage polarization through NF-κB signaling pathway. *Bioact. Mater.* **5**, 880–890 (2020).
44. J. E. Sero, H. Z. Sailem, R. C. Ardy, H. Almuttaqi, T. Zhang, C. Bakal, Cell shape and the microenvironment regulate nuclear translocation of NF-κB in breast epithelial and tumor cells. *Mol. Syst. Biol.* **11**, 790 (2015).
45. M. G. Dorrington, I. D. C. Fraser, NF-κB signaling in macrophages: Dynamics, crosstalk, and signal integration. *Front. Immunol.* **10**, 705 (2019).
46. H. Yu, L. Lin, Z. Zhang, H. Zhang, H. Hu, Targeting NF-κB pathway for the therapy of diseases: Mechanism and clinical study. *Signal Transduct. Target. Ther.* **5**, 209 (2020).
47. C. B. Phelps, R. R. Wang, S. S. Choo, R. Gaudet, Differential regulation of TRPV1, TRPV3, and TRPV4 sensitivity through a conserved binding site on the ankyrin repeat domain. *J. Biol. Chem.* **285**, 731–740 (2010).
48. A. M. Bagnell, C. J. Sumner, B. A. McCray, TRPV4: A trigger of pathological RhoA activation in neurological disease. *Bioessays* **44**, e2100288 (2022).
49. O. V. Savinova, A. Hoffmann, G. Ghosh, The Nfkb1 and Nfkb2 proteins p105 and p100 function as the core of high-molecular-weight heterogeneous complexes. *Mol. Cell* **34**, 591–602 (2009).
50. V. Tergaonkar, V. Bottero, M. Ikawa, Q. Li, I. M. Verma, IκB kinase-independent IκBα degradation pathway: Functional NF-κB activity and implications for cancer therapy. *Mol. Cell. Biol.* **23**, 8070–8083 (2003).
51. S. O. Rahaman, L. M. Grove, S. Paruchuri, B. D. Southern, S. Abraham, K. A. Niese, R. G. Scheraga, S. Ghosh, C. K. Thodeti, D. X. Zhang, M. M. Moran, W. P. Schilling, D. J. Tschumperlin, M. A. Olman, TRPV4 mediates myofibroblast differentiation and pulmonary fibrosis in mice. *J. Clin. Invest.* **124**, 5225–5238 (2014).
52. K. C. Barnett, J. M. Coronas-Serna, W. Zhou, M. J. Ernandes, A. Cao, P. J. Kranzusch, J. C. Kagan, Phosphoinositide interactions position cGAS at the plasma membrane to ensure efficient distinction between self- and viral DNA. *Cell* **176**, 1432–1446.e11 (2019).
53. Y. Ji, Y. Luo, Y. Wu, Y. Sun, L. Zhao, Z. Xue, M. Sun, X. Wei, Z. He, S. A. Wu, L. L. Lin, Y. Lu, L. Chang, F. Chen, S. Chen, W. Qian, X. Xu, S. Chen, D. Pan, Z. Zhou, S. Xia, C. C. A. Hu, T. Liang, L. Qi, SEL1L–HRD1 endoplasmic reticulum-associated degradation controls STING-mediated innate immunity by limiting the size of the activable STING pool. *Nat. Cell Biol.* **25**, 726–739 (2023).
54. A. M. Rodgers, J. Lindsay, A. Monahan, A. V. Dubois, A. A. Faniyi, B. J. Plant, M. A. Mall, M. B. Ekkelenkamp, S. Elborn, R. J. Ingram, Biologically relevant murine models of chronic *Pseudomonas aeruginosa* respiratory infection. *Pathogens* **12**, 1053 (2023).

Acknowledgments: We would like to acknowledge J. Qin at Lerner Research Institute for input on the protein structural work in this manuscript. We would like to acknowledge A. Attaway for the use of BioRender license. We would also like to acknowledge T. Stappenbeck at Lerner Research Institute for critically reading the manuscript. **Funding:** This work was supported by the National Institutes of Health grant K08-HL133380 (R.G.S.), National Institutes of Health grant R01-HL155064 (R.G.S.), National Institutes of Health grant R01-HL158746 (M.A.O.), National Institutes of Health grant R01-HL133721 (M.A.O.), and National Institutes of Health grant R35GM149240 (V.V.). **Author contributions:** Conceptualization: R.G.S., M.A.O., Y.W., L.M.G., and A.M.B. Methodology: Y.W. and R.G.S. Investigation: A.M.B., M.E.G., Y.W., E.M.O., Y.L., S.A., A.R., R.G.S., H.B., C.M.S., A.C.-B., and V.V. Visualization: A.M.B., M.E.G., R.G.S., and E.M.O. Funding acquisition: R.G.S. Project administration: R.G.S. Supervision: R.G.S. Writing—original draft: A.M.B., M.E.G., E.M.O., and R.G.S. Writing—review and editing: A.M.B., M.E.G., E.M.O., M.A.O., R.G.S., and C.M.S. **Competing interests:** The authors declare that they have no competing interests. **Data and materials availability:** Datasets for the scRNA-seq data are deposited in the NIH NCBI GEO (https://ncbi.nlm.nih.gov/geo/query/acc.cgi?acc=GSE295714). All other data needed to evaluate the conclusions in the paper are present in the paper or the Supplementary Materials. Reagents can be shared with the appropriate material transfer agreement (MTA).

Submitted 13 September 2024
Resubmitted 8 June 2025
Accepted 21 November 2025
Published 23 December 2025
10.1126/scisignal.adt1539